

## Enhanced hydrogen storage kinetics of nanocrystalline and amorphous Mg<sub>2</sub>N-type alloy by substituting Ni with Co

ZHANG Yang-huan<sup>1,2</sup>, SONG Chun-hong<sup>1,2</sup>, REN Hui-ping<sup>2</sup>,  
LI Zhi-gang<sup>1,2</sup>, HU Feng<sup>1,2</sup>, ZHAO Dong-liang<sup>1</sup>

1. Department of Functional Material Research, Central Iron and Steel Research Institute, Beijing 100081, China;
2. Elected State Key Laboratory, Inner Mongolia University of Science and Technology, Baotou 014010, China

Received 15 September 2010; accepted 29 November 2010

**Abstract:** In order to improve the hydrogen storage kinetics of the Mg<sub>2</sub>Ni-type alloys, Ni in the alloy was partially substituted with element Co. The Mg<sub>2</sub>Ni-type Mg<sub>2</sub>Ni<sub>1-x</sub>Co<sub>x</sub> (x=0, 0.1, 0.2, 0.3, 0.4) alloys were fabricated by melt-spinning technique. The structures of the as-spun alloys were characterized by XRD and TEM. The gaseous and electrochemical hydrogen storage kinetics of the alloys was measured. The results show that the substitution of Co for Ni notably enhances the glass forming ability of the Mg<sub>2</sub>Ni-type alloy. The amorphization degree of the alloys visibly increases with rising of Co content. Furthermore, the substitution of Co for Ni significantly improves the hydrogen storage kinetics of the alloys. With an increase in the amount of Co substitution from 0 to 0.4, the hydrogen absorption saturation ratio of the as-spun (15 m/s) alloy increases from 81.2% to 84.9%, the hydrogen desorption ratio from 17.60% to 64.79%, the hydrogen diffusion coefficient increases from  $1.07 \times 10^{-11}$  to  $2.79 \times 10^{-11}$  cm<sup>2</sup>/s and the limiting current density increases from 46.7 to 191.7 mA/g, respectively.

**Key words:** Mg<sub>2</sub>Ni-type alloy; substituting Ni with Co; melt spinning; hydrogen storage kinetics

### 1 Introduction

Mg<sub>2</sub>Ni-type intermetallic compounds are intensively studied because they are expected to be used as hydrogen storage materials [1] or negative electrode in Ni-MH batteries [2]. However, their practical application to hydrogen suppliers has been limited mainly due to their sluggish hydriding/dehydriding kinetics as well as high thermodynamic stability of their corresponding hydride. Therefore, a variety of attempts, mechanical alloying (MA) [3], melt spinning [4–5], surface modification [6], adding catalysts [7], hydriding combustion synthesis [8], GPa hydrogen pressure method [9], gravity casting [10], alloying with other elements [11], spark plasma sintering [12] etc, have been developed to enhance their hydriding/dehydriding kinetics and to reduce their thermodynamic stability. It was documented that the researches in this area have achieved great improvements in the hydrogen absorption/desorption kinetics of the Mg-based alloys.

However, the key challenge about the reduction in thermodynamic stability of Mg-based hydrides still remains intact.

High energy ball-milling is regarded as a quite powerful method for the fabrication of nanocrystalline and amorphous Mg and Mg-based alloys. Especially, it is the most appropriate method to solubilize particular elements into MgH<sub>2</sub> or Mg<sub>2</sub>NiH<sub>4</sub> above the thermodynamic equilibrium limit, facilitating the destabilization of MgH<sub>2</sub> or Mg<sub>2</sub>NiH<sub>4</sub> [13]. However, the milled Mg<sub>2</sub>Ni-type alloy electrodes exhibit extremely poor electrochemical cycle stability owing to the disappearance of the metastable structures formed by ball milling during the multiple electrochemical charging and discharging cycles [14], which is an insurmountable bottleneck for its practical application as the electrode materials.

On the contrary, the melt-spun treatment may inhibit the sharp degradation of the hydrogen absorbing and desorbing cyclic characteristics of Mg-based compounds [15]. Furthermore, the melt-spinning

**Foundation item:** Projects (50871050, 50961009) supported by the National Natural Science Foundation of China; Projects (2010ZD05, 2011ZD10) supported by Natural Science Foundation of Inner Mongolia, China; Project (NJzy08071) supported by High Education Science Research Project of Inner Mongolia, China

**Corresponding author:** ZHANG Yang-huan; Tel: +86-10-62187570; E-mail: [zyh59@yahoo.com.cn](mailto:zyh59@yahoo.com.cn)  
DOI: 10.1016/S1003-6326(11)60963-1

technique is an important method to produce a nanocrystalline structure and has been regarded to be the most appropriate for the mass-production of the nanocrystalline Mg-based alloys. The alloys, possessing the nanocrystalline and amorphous structure produced by melt-spinning method, exhibit excellent initial electrochemical hydrogen storage characteristics similar to those of the alloys fabricated by the MA process. SPASSOV and KÖSTER [16] have prepared  $Mg_2(Ni,Y)$  hydrogen storage alloy with the composition of  $Mg_{63}Ni_{30}Y_7$  by rapid solidification process, exhibiting a maximum hydrogen absorption capacity of about 3.0%. In addition, the melt-spun  $Mg_2(Ni,Y)$  alloys have demonstrated an enhanced hydrogenation kinetics compared with those of the conventionally prepared polycrystalline  $Mg_2Ni$  alloys, to be comparable to that of the nanocrystalline ball-milled  $Mg_2Ni$ . HUANG et al [17] have concluded that the amorphous and nanocrystalline Mg-based alloy  $(Mg_{60}Ni_{25})_{90}Nd_{10}$  prepared by melt-spinning technique displays the highest discharge capacity of 580 mA·h/g.

In the present work, the Mg-Ni-based  $Mg_2Ni_{1-x}Co_x$  ( $x=0-0.4$ ) nanocrystalline and amorphous alloys have been synthesized by melt-spinning technology. Moreover, the effects of substituting Ni with Co on the structures and hydrogen storage kinetics of the alloys were investigated in detail.

## 2 Experimental

The nominal compositions of the experimental alloys were  $Mg_2Ni_{1-x}Co_x$  ( $x=0, 0.1, 0.2, 0.3, 0.4$ ). For convenience, the alloys were denoted with Co content as  $Co_0, Co_{0.1}, Co_{0.2}, Co_{0.3}$  and  $Co_{0.4}$ , respectively. The experimental alloys were prepared by using a vacuum induction furnace in a helium atmosphere at a pressure of 0.04 MPa. A part of the as-cast alloys were re-melted and spun by melt-spinning with a rotating copper roller cooled by water. The spinning rate was approximately expressed by the linear velocity of the copper roller. The spinning rates used in the experiment were 15, 20, 25 and 30 m/s, respectively.

The phase structures of the as-cast and spun alloys were determined by X-ray diffraction (XRD) (D/max/2400). The diffraction, with the experimental parameters of 160 mA, 40 kV and 10 (°)/min, respectively, was performed with Cu  $K_{\alpha 1}$  radiation filtered by graphite. The effective crystal sizes were calculated from Scherrer's formula [18].

The thin film samples of the as-spun alloys were prepared by ion etching method in order to observe the morphology with high resolution transmission electron microscope (HRTEM) (JEM-2100F, operated at 200 kV), and also to determine the crystalline state of the samples

with electron diffraction (ED). The average grain size of the as-spun alloys was measured by a linear intercept method on the HRTEM micrographs.

The hydrogen absorption and desorption kinetics of the alloys was measured by an automatically controlled Sieverts apparatus. Prior to measuring the hydriding and dehydriding kinetics of the alloys, several hydrogen absorbing and desorbing cycles were performed in order to activate the materials. The hydrogen absorption was conducted at 1.5 MPa and 200 °C, and the hydrogen desorption was conducted at a pressure of  $1 \times 10^{-4}$  MPa and 200 °C.

The alloy ribbons were pulverized into fine powder of about 20  $\mu m$  by mechanical milling and then mixed with carbonyl nickel powder in a mass ratio of 1:4. The mixture was cold pressed under a pressure of 35 MPa into round electrode pellets of 10 mm in diameter and total mass of about 1 g. The electrochemical hydrogen storage kinetics of the alloy electrodes was tested by a tri-electrode open cell, consisting of a metal hydride electrode, a sintered  $NiOOH/Ni(OH)_2$  counter electrode and a Hg/HgO reference electrode. The electrolyte is a solution of 6 mol/L KOH. The voltage between the negative electrode and the reference electrode was defined as the discharge voltage. In every cycle, the alloy electrode was first charged at a constant current density, and following the resting for 15 min, it was discharged at the same current density to cut-off voltage of  $-0.500$  V. The environment temperature of the measurement was kept at 30 °C.

The electrochemical impedance spectra (EIS) and the Tafel polarization curves of the alloys were measured using an electrochemical workstation (PARSTAT 2273). The fresh electrodes were fully charged and then rested for 2 h up to the stabilization of the open circuit potential. The EIS spectra of the alloy electrodes were measured in the frequency range from 10 kHz to 5 mHz at 50% depth of discharge (DOD). The Tafel polarization curves were measured in the potential range of  $-1.2$  to  $1.0$  V (vs Hg/HgO) with a scan rate of 5 mV/s. For the potentiostatic discharge, the test electrodes in the fully charged state were discharged at 500 mV potential steps for 4 500 s on electrochemical workstation (PARSTAT 2273), using the CorrWare electrochemistry corrosion software.

## 3 Results and discussion

### 3.1 Structural characteristics

The XRD profiles of the as-spun (15 and 25 m/s) alloys are presented in Fig. 1. It is evident that the as-spun alloys have a multiphase structure, comprising of a major phase  $Mg_2Ni$  and secondary phases  $MgCO_2$  and Mg, and the amount of these secondary phases obviously

increases with rising of Co content. The melt-spinning treatment has an unapparent influence on the structure of the  $\text{Co}_0$  alloy, while it causes a great change of the structure of the  $\text{Co}_{0.4}$  alloy. As the spinning rate reaches 25 m/s, the  $\text{Co}_{0.4}$  alloy exhibits an obvious amorphous structure. Therefore, it may be surmised that the substitution of Co for Ni facilitates the glass formation in the  $\text{Mg}_2\text{Ni}$ -type alloy. Two possibilities may be considered the reasons for the above result. Firstly, the addition of the third element to Mg-Ni or Mg-Cu alloys significantly facilitates the glass-formation [19]. Secondary, the glass forming ability of an alloy is closely related to the difference of the atomic radii in the alloy. The higher difference of the atomic radii enhances the glass forming ability [20]. Therefore, the much larger atomic radius of Co compared with that of Ni facilitates the glass-formation. The lattice parameters, cell volumes and full width at half maximum (FWHM) values of the main diffraction peaks of the as-spun alloys are listed in Table 1, which were calculated by using Jade 6.0 software. It is derived in Table 1 that increasing the amount of Co substitution causes not only an visible increase in the FWHM values of the main diffraction

peaks of the as-spun alloys but also an evident enlargement in the lattice parameters and cell volume of the alloys, which is attributed to the larger atomic radius of Co than Ni. Based on the FWHM values of the broad diffraction peak (203) in Fig. 1, the grain sizes  $\langle D_{hkl} \rangle$  (Å) of the as-spun alloys are calculated using Scherrer's equation, and also listed in Table 1. It reveals that the substitution of Co for Ni causes an obvious reduction of the grain sizes of the alloys. It must be mentioned that the data in Fig. 1(b) and Table 1 corresponding to the spinning rate of 25 m/s are from Ref. [21].

The TEM micrographs and ED patterns of the as-spun (25 m/s) alloys are shown in Fig. 2. It can be seen that the as-spun  $\text{Co}_{0.1}$  alloy displays a nearly complete nanocrystalline structure, and its electron diffraction (ED) pattern displays sharp multi-haloes, corresponding to a crystalline structure, while the  $\text{Co}_{0.4}$  alloy exhibits a clear feature of the nanocrystalline embedded in the amorphous matrix, and its electron diffraction pattern consists of broad and dull halo, confirming the presence of an amorphous structure. It is quite evident that the amorphization degree of the as-spun alloys visibly increases with the increase in the

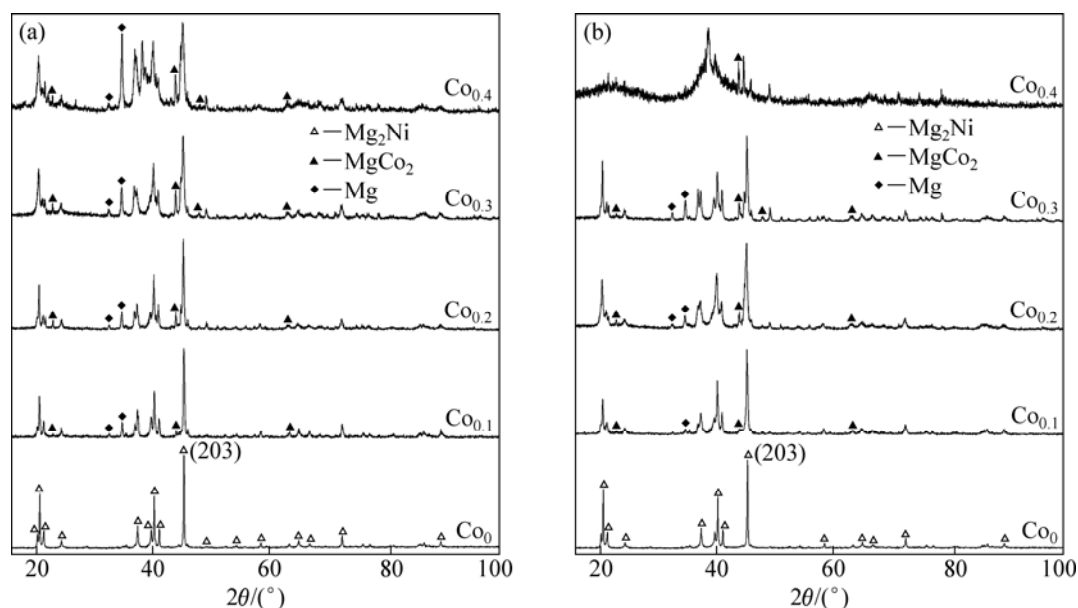
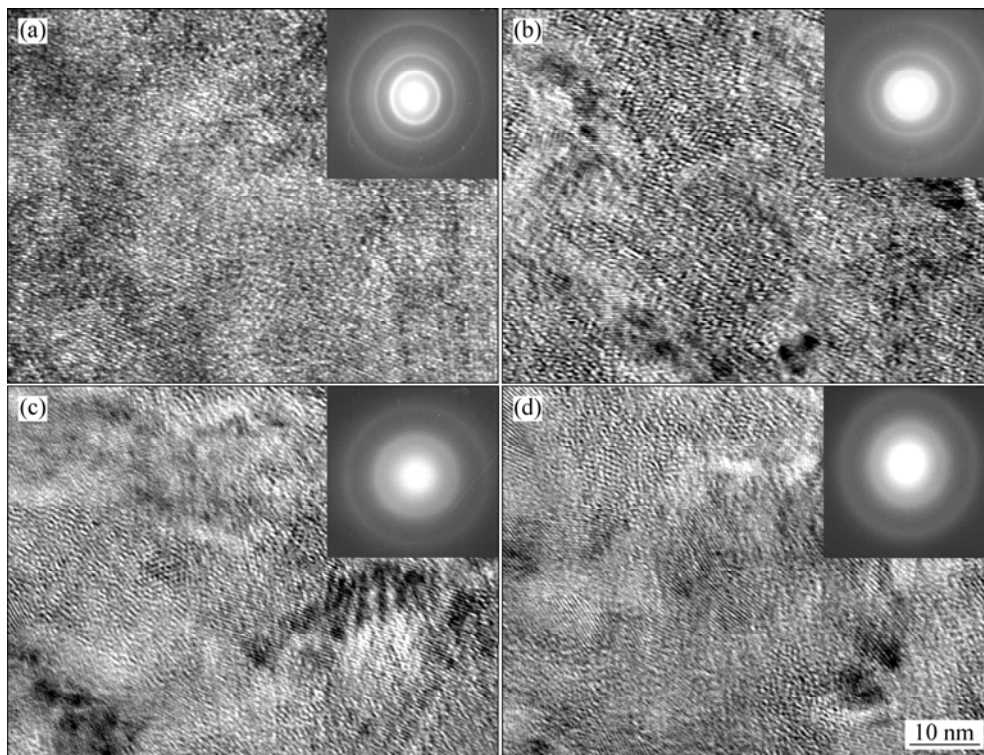


Fig. 1 XRD patterns of as-spun alloys: (a) 15 m/s; (b) 25 m/s

Table 1 Lattice parameters, cell volumes, FWHM values and grain sizes of as-spun alloys

Alloy	FWHM value ( $2\theta=45.14^\circ$ )		Grain size $D_{203}/\text{nm}$		Lattice parameter and cell volume					
	15 m/s	25 m/s	15 m/s	25 m/s	a/nm		c/nm		$V/\text{nm}^3$	
					15 m/s	25 m/s	15 m/s	25 m/s	15 m/s	25 m/s
$\text{Co}_0$	0.171	0.179	50	48	0.5210	0.5211	1.3251	1.3265	0.3115	0.3119
$\text{Co}_{0.1}$	0.191	0.310	45	27	0.5213	0.5219	1.3256	1.3318	0.3120	0.3141
$\text{Co}_{0.2}$	0.265	0.425	32	20	0.5217	0.5225	1.3305	1.3323	0.3136	0.3150
$\text{Co}_{0.3}$	0.357	0.461	24	18	0.5224	0.5226	1.3312	1.3401	0.3146	0.3170
$\text{Co}_{0.4}$	0.449	—	19	—	0.5224	—	1.3318	—	0.3147	—



**Fig. 2** HRTEM micrographs and ED patterns of as-spun (25 m/s) alloy: (a)  $\text{Co}_{0.1}$  alloy; (b)  $\text{Co}_{0.2}$  alloy; (c)  $\text{Co}_{0.3}$  alloy; (d)  $\text{Co}_{0.4}$  alloy

amount of Co substitution, which conforms to the XRD observations depicted in Fig. 1.

### 3.2 Hydrogen absorption and desorption kinetics

The hydrogen absorption was carried out under hydrogen pressure of 1.5 MPa (in fact, this pressure is initial pressure of hydriding process), and hydrogen desorption was carried out in an initial pressure of  $1 \times 10^{-4}$  MPa at 200 °C. Our previous work [22] has revealed that crystallization temperatures of the as-spun alloys are higher than 200 °C, suggesting that there is not an obvious change of the phase structure of the alloy at the hydriding and dehydriding temperature.

The hydrogen absorption kinetics of the alloy is signified by hydrogen absorption saturation ratio ( $R_t^a$ ), defined as  $R_t^a = C_t^a / C_{100}^a \times 100\%$ , where  $C_{100}^a$  and  $C_t^a$  are hydrogen absorption capacities in the time of 100 min and  $t$  min, respectively. Apparently, for a fixed time  $t$ , a larger saturation ratio  $R_t^a$  means better hydrogen absorption kinetics. The experimental result indicates that, for all the experimental alloys, the  $C_{100}^a$  values are more than 98% of their saturated hydrogen absorption capacities. Therefore, it is reasonable to take the  $C_{100}^a$  value as the saturated hydrogen absorption capacity of the alloy. The evolution of the hydrogen absorption saturation ratio ( $R_5^a$ ) ( $t=5$ ) of the alloys with Co content is presented in Fig. 3. It is evident that all the as-spun alloys exhibit superior hydrogen absorption

kinetics. The substitution of Co for Ni notably enhances the  $R_5^a$  values of the alloys, but the positive function of Co substitution on hydrogen absorption kinetics clearly reduces with rising of spinning rate. It is noteworthy that, as Co content increases to 0.4, the substitution of Co for Ni leads to a slight decline of the  $R_5^a$  values of the alloys, but the  $R_5^a$  values of the alloys substituted by Co always are higher than those of the Co-free alloys, confirming that thus substitution improves the hydrogen absorption kinetics of the as-cast and spun  $\text{Mg}_2\text{Ni}$ -type alloys. The slight decrease in the  $R_5^a$  value of the alloy induced by superfluous Co substitution ( $x=0.4$ ) is probably ascribed

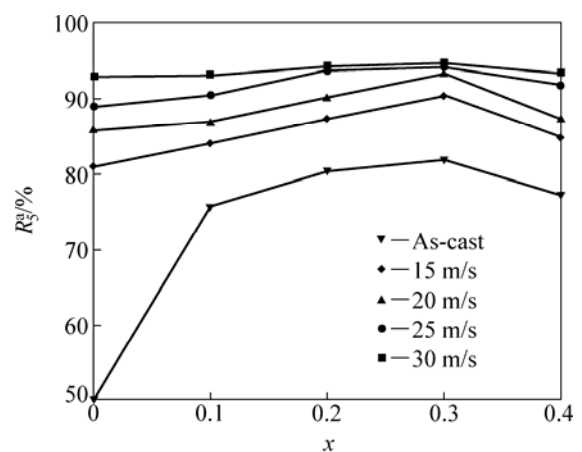


**Fig. 3** Evolution of hydrogen absorption saturation ratio ( $R_5^a$ ) of alloys with Co content

to the formation of secondary phases  $\text{MgCo}_2$  and  $\text{Mg}$  created by thus substitution. The convincing mechanism needs to be investigated further.

The improved hydrogen absorption kinetics can be explained with the enhanced hydrogen diffusivity in the amorphous and nanocrystalline microstructures as the amorphous phase around the nanocrystalline leads to an easier access of hydrogen to the nanograins, avoiding the long-range diffusion of hydrogen through an already formed hydride, which is often the slowest stage of absorption. Upon refining the microstructure, a lot of new crystallites and grain boundaries evolve, which may act as fast diffusion paths for hydrogen absorption [23].

Similarly, the hydrogen desorption kinetics of the alloy is indicated by hydrogen desorption ratio ( $R_t^d$ ), defined as  $R_t^d = C_t^d / C_{100}^a \times 100\%$ , where  $C_{100}^a$  is the hydrogen absorption capacity in 100 min and  $C_t^d$  is the hydrogen desorption capacity in the time of  $t$  min, respectively. The hydrogen desorption ratio ( $R_{20}^d$ ) of the alloys as a function of the Co content is depicted in Fig. 4. It can be seen from Fig. 4 that the substitution of Co for Ni visibly enhances the  $R_{20}^d$  values of the alloys, suggesting that thus substitution facilitates hydrogen desorption of  $\text{Mg}_2\text{Ni}$ -type alloy. With the increase in the amount of Co substitution from 0 to 0.4, the  $R_{20}^d$  value increases from 3.43% to 54.47% for the as-cast alloys, and from 26.1% to 70.19% for the as-spun (30 m/s) alloys. It must be mentioned that, for a fixed Co content, the  $R_{20}^d$  value of the alloy markedly grows with the increase of the spinning rate.

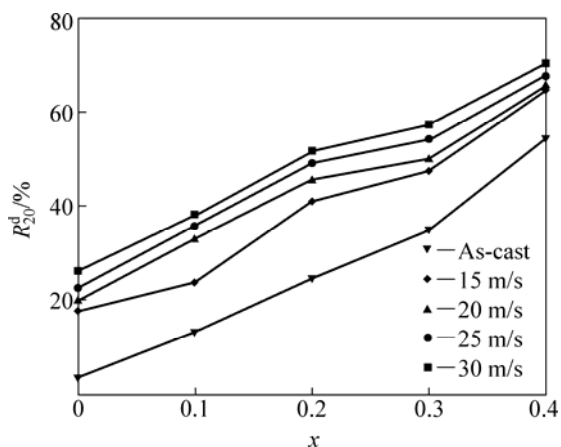


**Fig. 4** Evolution of hydrogen desorption ratio ( $R_{20}^d$ ) of alloys with Co content

It is well known that the hydrogen desorption kinetics of the alloy primarily relies on the hydrogen diffusion ability as well as the thermal stability of its hydride. The increased hydrogen desorption kinetics by Co substitution is ascribed to two reasons. Firstly, the substitution of Co for Ni notably intensifies the glass forming ability of  $\text{Mg}_2\text{Ni}$ -type alloy because amorphous

$\text{Mg}_2\text{Ni}$  shows an excellent hydrogen desorption capability. Secondly, such substitution decreases the stability of the hydride and makes the desorption reaction easier [24].

### 3.3 Electrochemical hydrogen storage kinetics

Electrochemical galvanostatic charge/discharge is a more effective and less time-consuming method for determining the hydrogen storage kinetics than a gaseous technique. It is quite important to restrict the rapid attenuation in the discharge capacity even at a high charge/discharge current density for the practical application of hydride electrode in Ni-MH battery. Generally, the electrochemical kinetics of the alloy is characterized by its high rate discharge ability (HRD), calculated according to following formula:  $\text{HRD} = C_{i,\text{max}} / C_{20,\text{max}} \times 100\%$ , where  $C_{i,\text{max}}$  and  $C_{20,\text{max}}$  are the maximum discharge capacities of the alloy electrode charged-discharged at the current densities of  $i$  and 20 mA/g, respectively.

The evolution of the HRD values of the as-spun (15 and 25 m/s) alloys with the discharge current density is illustrated in Fig. 5. It indicates that the HRD values of all the alloys increase with rising of Co content. As Co

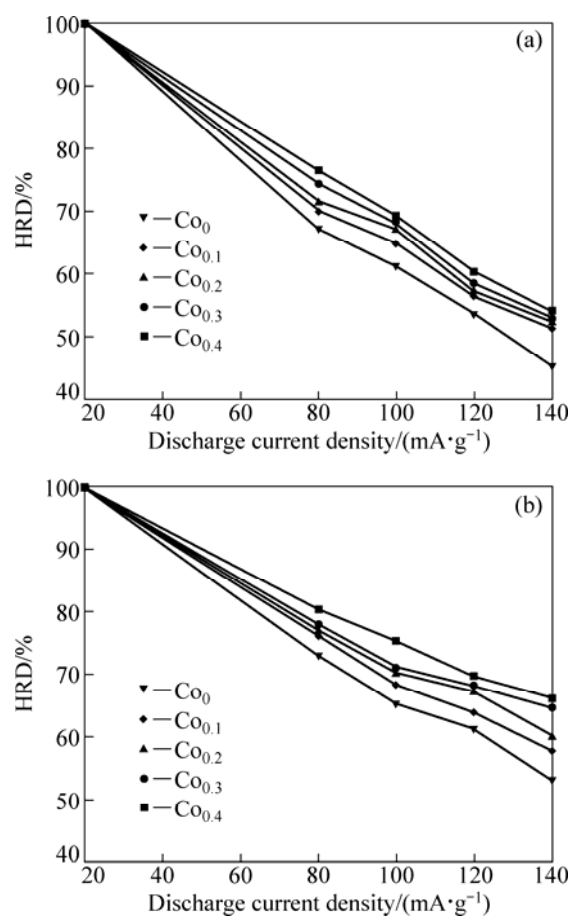


**Fig. 5** Evolution of high rate discharge ability (HRD) of alloys with discharge current density: (a) 15 m/s, (b) 25 m/s

content rises from 0 to 0.4, the HRD value ( $i=100$  mA/g) increases from 61.2% to 69.0% for the as-spun (15 m/s) alloys, and from 65.3% to 71.1% for the as-spun (25 m/s) alloys.

In order to reveal the mechanism of Co substitution improving hydrogen absorption kinetics of the alloy, it evidently is necessary to determine the influence of Co substitution on H diffusion ability in the alloy. Figure 6 shows the semilogarithmic curves of anodic current versus working duration of the as-spun (15 m/s) alloys. The diffusion coefficient  $D$  of the hydrogen atoms in the bulk of the alloy can be calculated through the slope of the linear region of the corresponding plots according to the following formulae [25]:

$$\lg i = \lg \left( \pm \frac{6FD}{da^2} (C_0 - C_s) \right) - \frac{\pi^2}{2.303} \frac{D}{a^2} t \quad (1)$$

$$D = - \frac{2.303a^2}{\pi^2} \frac{d \lg i}{dt} \quad (2)$$

where  $i$  is the diffusion current density (A/g);  $D$  is the hydrogen diffusion coefficient ( $\text{cm}^2/\text{s}$ );  $C_0$  is the initial hydrogen concentration in the bulk of the alloy ( $\text{mol}/\text{cm}^3$ );  $C_s$  is the hydrogen concentration on the surface of the alloy particles ( $\text{mol}/\text{cm}^3$ );  $a$  is the alloy particle radius (cm);  $d$  is the density of the hydrogen storage alloy ( $\text{g}/\text{cm}^3$ );  $t$  is the discharge time (s), respectively. The  $D$  values calculated by Eq. (2) are also presented in Fig. 6. It can be seen that  $D$  value increases with the increase in the Co content. As the amount of Co substitution rises from 0 to 0.4, the  $D$  value of the as-spun (15 m/s) alloy increases from  $1.07 \times 10^{-11}$  to  $2.79 \times 10^{-11} \text{ cm}^2/\text{s}$ .

High rate discharge ability (HRD) is a kinetic performance of hydrogen absorbing/desorbing of the alloy electrode, basically depending on the charge transfer at the alloy-electrolyte interface, the hydrogen diffusion process from the interior of the bulk to the surface of alloy particle [26]. The substitution of Co for Ni visibly enhances the HRD values of the alloys, which is attributed to a positive action of Co substitution on the hydrogen diffusion in the alloy. Furthermore, Co substitution accelerates the formation of a concentrated metallic Ni layer on the surface of the alloy electrode which is highly beneficial to enhance electrochemical catalytic property and to improve the reaction rate of hydrogen [26].

Figure 7 shows the electrochemical impedance spectra (EIS) of the as-spun (15 m/s) alloy electrodes at 50% DOD. It shows that each EIS spectrum contains two semicircles followed by a straight line. According to KURIYAMA et al [27], the smaller semicircle in the high frequency region is attributed to the contact

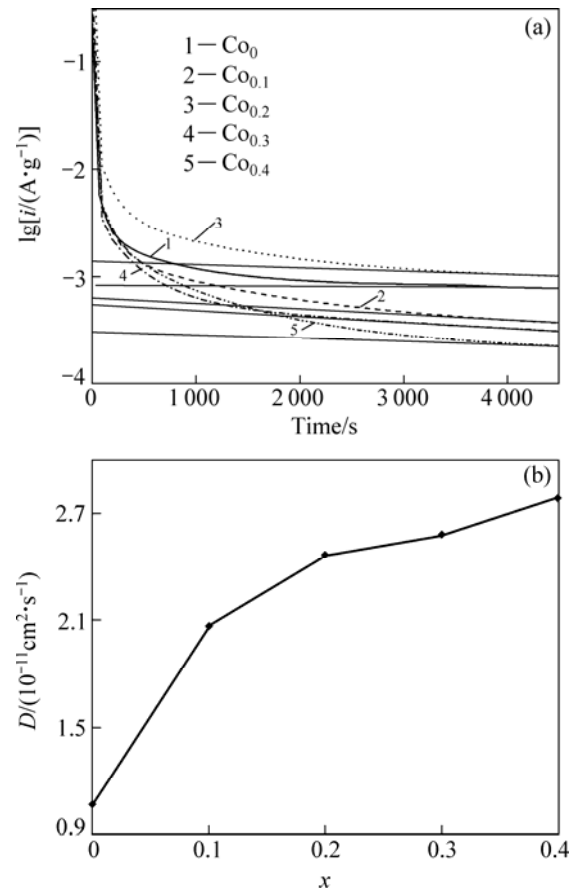


Fig. 6 Semilogarithmic curves of anodic current density vs time (a) and  $D$  vs  $x$  (b) of as-spun (15 m/s) alloys

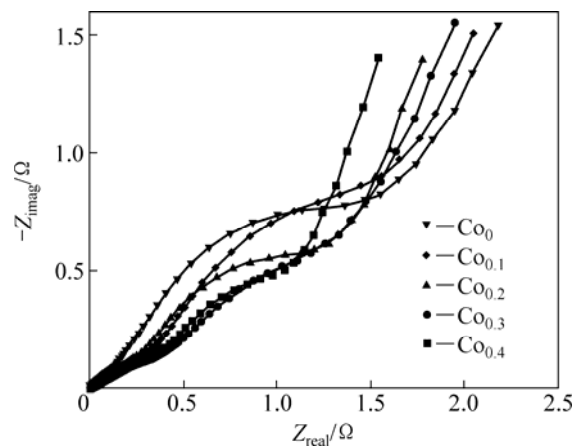
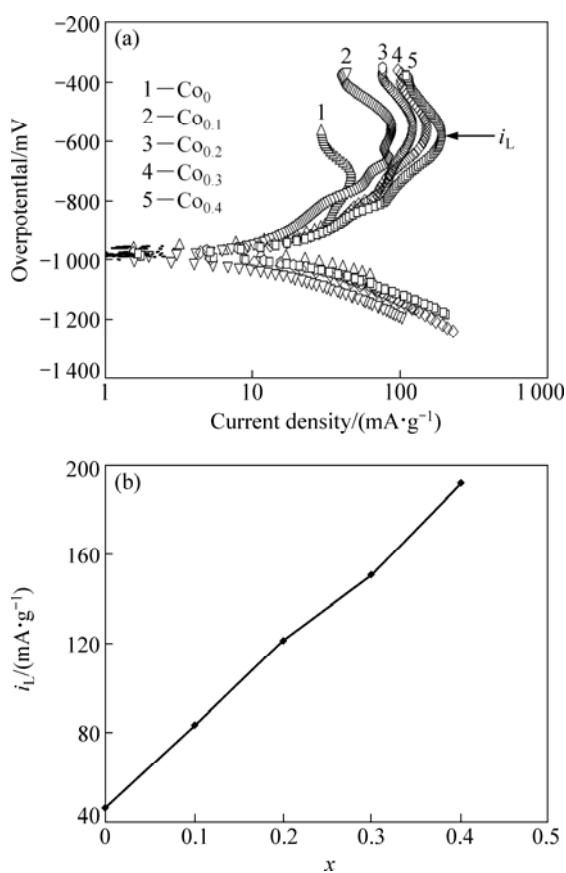


Fig. 7 Electrochemical impedance spectra (EIS) of as-spun (15 m/s) alloy electrodes at 50% depth of discharge (DOD)

resistance between the alloy powder and the conductive material, while the larger semicircle in the low frequency region is attributed to the charge-transfer resistance on the alloy surface. The linear response at low frequencies is indicative of hydrogen diffusion in the bulk alloy. Hence, the electrode kinetics of the as-spun alloys is dominated a mixed rate-determining process. It can be

seen from Fig. 7 that the radius of the large semicircle in the low frequency visibly decreases with increasing Co content, implying that the refined grain by Co substitution facilitates charge-transfer of the alloy electrode.

To determine the kinetics of hydrogen absorption/desorption, Tafel polarization measurements were carried out on the experimental alloy electrodes. Figure 8 shows the Tafel polarization curves of the as-spun (15 m/s) alloy electrodes at the 50% DOD. It indicates that, in all cases, the anodic current densities increase to a limiting value, then decrease. The existence of a limiting current density,  $i_L$ , suggests forming an oxidation layer on the surface of the alloy electrode, which resists further penetration of hydrogen atoms [28]. The decrease of the anodic charge current density on cycling implies that charging is becoming more difficult. Hence, the limiting current density,  $i_L$ , may be regarded as a critical passivation current density. The limiting current density  $i_L$  obtained from the Tafel polarization curves is also presented in Fig. 8. It can be seen from Fig. 8 that  $i_L$  values of the alloys notably increase with rising of Co content. With an increase in Co content from 0 to 0.4, the  $i_L$  value of the as-spun (15 m/s) alloy increases from 46.7 to 191.7 mA/g, indicating a higher



**Fig. 8** Tafel polarization curves of as-spun (15 m/s) alloy electrodes at 50% DOD (a) and evolution of limiting current density ( $i_L$ ) with Co content (b)

rate of hydrogen diffusion caused by substituting Ni with Co.

Based on the mentioned above, it can be concluded that the substitution of Co for Ni produces a significant improvement on the hydrogen storage kinetics of Mg<sub>2</sub>Ni-type alloy. However, it must be pointed out that the action mechanism of Co substitution is directly associated with the preparation technology of the alloy.

## 4 Conclusions

1) The nanocrystalline and amorphous Mg<sub>2</sub>Ni<sub>1-x</sub>Co<sub>x</sub> ( $x=0, 0.1, 0.2, 0.3, 0.4$ ) alloy ribbons are successfully fabricated by melt-spinning technology. The result indicates that the substitution of Co for Ni facilitates the glass formation in the Mg<sub>2</sub>Ni-type alloy. And the amorphization degree of the alloys visibly increases with increasing Co content. Furthermore, the substitution of Co for Ni, instead of changing the major phase Mg<sub>2</sub>Ni in the alloy, leads to forming secondary phases MgCo<sub>2</sub> and Mg.

2) The substitution of Co for Ni significantly improves the hydrogen storage kinetics of the alloys. The hydrogen absorption saturation ratio and hydrogen desorption ratio as well as the high rate discharge ability increase with rising of Co content, for which the notable increase of the hydrogen diffusion coefficient along with the limiting current density and the obvious decline of the electrochemical impedance caused by Co substitution are basically responsible.

## References

- [1] JAIN I P, LAL C, JAIN A. Hydrogen storage in Mg: A most promising material [J]. *Int J Hydrogen Energy*, 2010, 35: 5133–5144.
- [2] ZHAO X Y, MA L Q. Recent progress in hydrogen storage alloys for nickel/metal hydride secondary batteries [J]. *Int J Hydrogen Energy*, 2009, 34: 4788–4796.
- [3] KWON S N, BAEK S H, MUMM D R, HONG S H, SONG M Y. Enhancement of the hydrogen storage characteristics of Mg by reactive mechanical grinding with Ni, Fe and Ti [J]. *Int J Hydrogen Energy*, 2008, 33: 4586–4592.
- [4] TANAKA K, MIWA T, SASAKI K, KURODA K. TEM studies of nanostructure in melt-spun Mg-Ni-La alloy manifesting enhanced hydrogen desorbing kinetics [J]. *J Alloys Comp*, 2009, 478: 308–316.
- [5] HUANG L J, TANG J G, WANG Y, LIU J X, WU D C. Effects of microstructure on the electrode properties of melt-spun Mg-based amorphous alloys [J]. *J Alloys Comp*, 2009, 485: 186–191.
- [6] JANOT R, DAROK X, ROUGIER A, AYMARD L, NAZRI G A, TARASCON J M. Hydrogen sorption properties for surface treated MgH<sub>2</sub> and Mg<sub>2</sub>Ni alloys [J]. *J Alloys Comp*, 2005, 404–406: 293–296.
- [7] XIE L, LIU Y, ZHANG X Z, QU J L, WANG Y T, LI X G. Catalytic effect of Ni nanoparticles on the desorption kinetics of MgH<sub>2</sub> nanoparticles [J]. *J Alloys Comp*, 2009, 482: 388–392.
- [8] LIU X F, ZHU Y F, LI L Q. Structure and hydrogenation properties of nanocrystalline Mg<sub>2</sub>Ni prepared by hydriding combustion

- synthesis and mechanical milling [J]. *J Alloys Comp*, 2008, 455: 197–202.
- [9] KYOI D, SAKAI T, KITAMURA N, UEDA A, TANASE S. Synthesis of FCC Mg-Ta hydrides using GPa hydrogen pressure method and their hydrogen-desorption properties [J]. *J Alloys Comp*, 2008, 463: 306–310.
- [10] SONG M Y, YIM C D, BAE J S, MUMMD D R, HONG S H. Preparation by gravity casting and hydrogen-storage properties of Mg-23.5 wt.%Ni-(5, 10 and 15 wt.%)La [J]. *J Alloys Comp*, 2008, 463: 143–147.
- [11] SHANG C X, BOUOUDINA M, SONG Y, GUO Z X. Mechanical alloying and electronic simulations of (MgH<sub>2</sub>+M) systems (M=Al, Ti, Fe, Ni, Cu and Nb) for hydrogen storage [J]. *Int J Hydrogen Energy*, 2004, 29: 73–80.
- [12] LIU J, SONG X P, PEI P, CHEN G L. Hydrogen storage performance of Mg-based composites prepared by spark plasma sintering [J]. *J Alloys Comp*, 2009, 486: 338–342.
- [13] LIANG G. Synthesis and hydrogen storage properties of Mg-based alloys [J]. *J Alloys Comp*, 2004, 370: 123–128.
- [14] SONG M Y, KWON S N, BAE J S, HONG S H. Hydrogen-storage properties of Mg-23.5Ni-(0 and 5)Cu prepared by melt spinning and crystallization heat treatment [J]. *Int J Hydrogen Energy*, 2008, 33: 1711–1718.
- [15] SAVYAK M, HIRNYJ S, BAUER H D, UHLEMANN M, ECKERT J, SCHULTZ L, GEBERT A. Electrochemical hydrogenation of Mg<sub>65</sub>Cu<sub>25</sub>Y<sub>10</sub> metallic glass [J]. *J Alloys Comp*, 2004, 364: 229–237.
- [16] SPASSOV T, KÖSTER U. Thermal stability and hydriding properties of nanocrystalline melt-spun Mg<sub>63</sub>Ni<sub>30</sub>Y<sub>7</sub> alloy [J]. *J Alloys Comp*, 1998, 279: 279–286.
- [17] HUANG L J, LIANG G Y, SUN Z B, WU D C. Electrode properties of melt-spun Mg-Ni-Nd amorphous alloys [J]. *J Power Sources*, 2006, 160: 684–687.
- [18] WILLIAMSON G K, HALL W H. X-ray line broadening from filed aluminium and wolfram [J]. *Acta Metall*, 1953, 1: 22–31.
- [19] INOUE A, MASUMOTO T. Mg-based amorphous alloys [J]. *Mater Sci Eng A*, 1993, 173: 1–8.
- [20] CHEN H S. Thermodynamic considerations on the formation and stability of metallic glasses [J]. *Acta Metall*, 1974, 22(12): 1505–1511.
- [21] ZHANG Y H, REN H P, LI B W, GUO S H, PANG Z G, WANG X L. Electrochemical hydrogen storage characteristics of nanocrystalline and amorphous Mg<sub>20</sub>Ni<sub>10-x</sub>Co<sub>x</sub>(x=0–4) alloys prepared by melt spinning [J]. *Int J Hydrogen Energy*, 2009, 35: 8144–8156.
- [22] ZHANG Y H, ZHAO D L, LI B W, QI Y, GUO S H, WANG X L. Hydrogen storage behaviours of nanocrystalline and amorphous Mg<sub>20</sub>Ni<sub>10-x</sub>Co<sub>x</sub> (x=0–4) alloys prepared by melt spinning [J]. *Trans Nonferrous Met Soc China*, 2010, 20: 405–411.
- [23] WU Y, HAN W, ZHOU S X, LOTOTSKY M V, SOLBERG J K, YARTYS V A. Microstructure and hydrogenation behavior of ball-milled and melt-spun Mg-10Ni-2Mm alloys [J]. *J Alloys Comp*, 2008, 466: 176–181.
- [24] TAKAHASHI Y, YUKAWA H, MORINAGA M. Alloying effects on the electronic structure of Mg<sub>2</sub>Ni intermetallic hydride [J]. *J Alloys Comp*, 1996, 242: 98–107.
- [25] ZHENG G, POPOV B N, WHITE R E. Electrochemical determination of the diffusion coefficient of hydrogen through a LaNi<sub>4.25</sub>Al<sub>0.75</sub> electrode in alkaline aqueous solution [J]. *J Electrochem Soc*, 1995, 142: 2695–2698.
- [26] GASIOROWSKI A, IWASIECZKO W, SKORYNA D, DRULIS H, JURCZYK M. Hydriding properties of nanocrystalline Mg<sub>2-x</sub>M<sub>x</sub>Ni alloys synthesized by mechanical alloying (M=Mn, Al) [J]. *J Alloys Comp*, 2004, 364: 283–288.
- [27] KURIYAMA N, SAKAI T, MIYAMURA H, UEHARA I, ISHIKAWA H, IWASAKI T. Electrochemical impedance and deterioration behavior of metal hydride electrodes [J]. *J Alloys Comp*, 1993, 202: 183–197.
- [28] NIU H, NORTHWOOD D, DEREK O. Enhanced electrochemical properties of ball-milled Mg<sub>2</sub>Ni electrodes [J]. *Int J Hydrogen Energy*, 2002, 27: 69–77.

## Co 替代 Ni 改善纳米晶和非晶 Mg<sub>2</sub>Ni 型合金的贮氢动力学

张羊换<sup>1,2</sup>, 宋春红<sup>1,2</sup>, 任慧平<sup>2</sup>, 李志刚<sup>1,2</sup>, 胡锋<sup>1,2</sup>, 赵栋梁<sup>1</sup>

1. 钢铁研究总院 功能材料研究所, 北京 100081;

2. 内蒙古科技大学 国家重点实验室培育基地, 包头 014010

**摘要:** 为了改善 Mg<sub>2</sub>Ni 型合金的贮氢动力学性能, 用 Co 部分替代合金中的 Ni, 用快淬技术制备了 Mg<sub>2</sub>Ni<sub>1-x</sub>Co<sub>x</sub> (x=0, 0.1, 0.2, 0.3, 0.4) 贮氢合金。用 XRD、HRTEM 表征了快淬态合金的微观结构, 用自动控制的 Sieverts 设备测试了合金的吸放氢动力学性能, 用程控电池测试仪测定了合金薄带的电化学贮氢动力学。结果表明: Co 替代 Ni 提高了 Mg<sub>2</sub>Ni 型合金的非晶形成能力, 合金的非晶化程度随着 Co 含量的增加而增加。此外, Co 替代 Ni 显著地改善了合金的贮氢动力学, 当 Co 含量从 0 增加到 0.4 时, 快淬态(15 m/s)合金在 5 min 内的吸氢饱和率从 81.2% 增加到 84.9%, 20 min 的放氢率从 17.60% 增加到 64.79%, 氢扩散系数从 1.07×10<sup>-11</sup> cm<sup>2</sup>/s 增加到 2.79×10<sup>-11</sup> cm<sup>2</sup>/s, 极限电流密度从 46.7 mA/g 增加到 191.7 mA/g。

**关键词:** Mg<sub>2</sub>Ni 型合金; Co 替代 Ni; 快淬; 贮氢动力学

(Edited by LI Xiang-qun)